Turbulence Measurements in Hypersonic Shock-Wave Boundary-Layer Interaction Flows

V. Mikulla* and C.C. Horstman†
NASA Ames Research Center, Moffett Field, Calif.

Turbulent intensity and Reynolds shear stress measurements are presented for two nonadiabatic hypersonic shock-wave boundary-layer interaction flows, one with and one without separation. These measurements were obtained using a new hot-wire probe specially designed for heated flows. Comparison of the separated and attached flows shows a significant increase above equilibrium values in the turbulent intensity and shear stress downstream of the interaction region for the attached case, while for the separated case, the turbulent fluxes remain close to equilibrium values. This effect results in substantial differences in turbulence lifetimes for the two flows. We propose that these differences are due to a coupling between the turbulent energy and separation bubble unsteadiness, a hypothesis supported by the statistical properties of the turbulent fluctuations.

Nomenclature

C_F = local skin friction coefficient $(\tau_w / \frac{1}{2}\bar{\rho}_\infty \bar{u}^2_\infty)$
c_p = specific heat at constant pressure
f = frequency
M = Mach number
p = pressure
Pr_t = Turbulent Prandtl number, see Eq. (4)
$R_{(\rho u)'v'}$ = correlation coefficient of mass-flux and vertical-velocity fluctuations $[(\rho u)'v']/[<(\rho u)'><v'>]$
T = temperature
u = axial velocity
v = vertical velocity
x = axial coordinate, distance from leading edge of shock-wave generator
x_0 = axial location of incident shock impingement on cylinder surface in the absence of a boundary layer
y = distance normal to model surface
α = shock-wave generator leading-edge angle
γ = ratio of specific heats
δ = boundary-layer thickness
δ_0 = boundary-layer thickness ahead of interaction
ρ = density
$\langle ( ) \rangle$ = root mean square

Superscripts

$( )'$ = fluctuating value
$\overline{( )}$ = time averaged

Subscripts

t = total or stagnation conditions
∞ = local freestream ahead of interaction

I. Introduction

WITH the rapid advance in computational fluid dynamics over the past few years, computations that were not feasible several years ago are now being performed routinely. While examples of successful computations of shock-wave boundary-layer interaction flows at supersonic speeds with modest pressure rises have recently been reported,[1-3] similar computations for hypersonic boundary layers with a large pressure rise and extensive separation have shown significant deviations from experimental observations in the interaction region.[4,5] Improved solutions to these strongly coupled viscous-inviscid flows are dependent on better turbulence modeling. To date, the development of new turbulence models for such flows has relied on comparing the numerical results, which incorporate these models with measured mean-flow quantities, and then iterating the models. Additional information has been gained through the use of approximate momentum and energy integral techniques using experimental mean-flow quantities to determine the turbulent stresses.[4] Although these techniques have been partially successful in suggesting model changes, the direct measurement of the turbulent fluxes would provide data which could be used for the direct confirmation of the turbulence models and perhaps, more importantly, provide additional insight into the physics of the problem. Unfortunately, with the exception of the Rose and Johnson data[6] for an unseparated supersonic shock-wave boundary-layer interaction flow, no fluctuating turbulence data exist for compressible interaction flows.

This paper describes a series of turbulence measurements which extend the work of Rose and Johnson[6] to include nonadiabatic hypersonic interaction flows. The measurements were made possible by new developments in hot-wire probe design. In addition, the present measurements were obtained for two shock-wave boundary-layer interaction flows, one with and one without separation, which permitted a direct comparison in order to determine the influence of separation on the fluctuating flowfield. A previous paper[4] describes the experimental mean-flow documentation and a numerical simulation employing the complete time-averaged Navier-Stokes equations, along with algebraic turbulence models for these two flows. The present measurements, which include detailed surveys of the turbulent intensities and the Reynolds shear stresses throughout the interaction regions, were obtained using new hot-wire probes and measurement techniques previously described in Ref. 7. The statistical properties of the fluctuating quantities were also obtained which provide new insight into the physics of turbulent boundary-layer separation. In particular, significant differences in the fluctuating quantities for the separated and nonseparated boundary layer were observed downstream of the two interaction regions. From these differences it became apparent that the separation process enhances the return of the boundary layer to an equilibrium condition.

Received August 25, 1975; revision received November 24, 1975. The authors wish to thank Fred Lemas, who was responsible for the design and construction of the new hot-wire probes.

Index categories: Supersonic and Hypersonic Flow; Boundary Layers and Convective Heat Transfer – Turbulent.

*National Research Council Associate; now Scientist, Messerschmitt-Bölkow-Blohm, Munich, West Germany.

†Assistant Chief, Experimental Fluid Dynamic Branch. Associate Fellow AIAA.

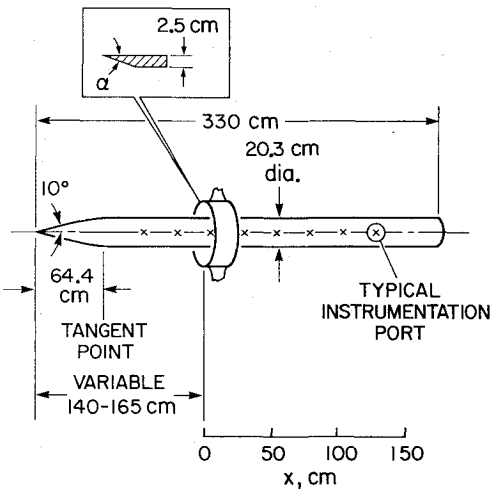

Fig. 1 Test model.

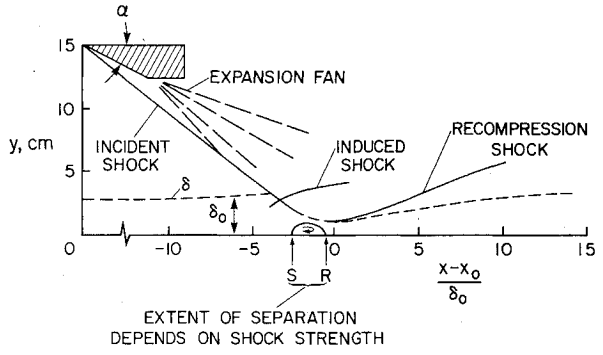

Fig. 2 Flowfield.

II. Description of Experiment

A. Wind Tunnel

The investigation was conducted in the Ames 3.5-ft hypersonic wind tunnel. This facility operates in a blowdown made and utilizes contoured axisymmetric nozzles to achieve a uniform Mach number in an approximately 0.7-m-diam, 4-m-long open-jet test core. The present tests were performed at a nominal freestream Mach number of 7.2, and with nominal values of total temperature and pressure of 695K and 34 atm.

B. Test Model and Flowfield

The test model consisted of a 20.3-cm-diam, 330-cm-long cone-ogive cylinder; its axis was aligned with the freestream flow (see Fig. . 1). Annular 51-cm-diam shock-wave generators, mounted concentric with the cylinder axis, were used to generate shock waves of two different strengths by beveling the sharp leading edge at either 7.5° or 15°. Figure 2 depicts the major features of the shock-wave, boundary-layer interaction zone. The incident shock wave, weakened and curved somewhat by the expansion fan emanating from the corner of the generator, impinges on the incoming boundary layer. The subsequent increases in surface pressure cause the boundary layer to thicken, or separate as in the case for the 15° generator, and induce a shock wave. Thereafter, rapid-flow turning and boundary-layer thinning occur and a recompression shock is formed. Previous results[4] have presented detailed surface and mean-flowfield measurements throughout the interaction region for both flowfields. The nominal measured boundary-layer parameters ahead of the interaction for the 7.5° (attached) and 15° generator angles were, respectively: edge Mach numbers, 6.7 and 6.9; boundary-layer thicknesses 3.2 cm and 2.7 cm; and Reynolds numbers based on boundary-layer thicknesses 0.23×10^6 and 0.20×10^6. The model wall temperature was 300 K. The extent of separation for the separated case was $(x-x_0)/\delta_0 = -3.15$ to -1.68.

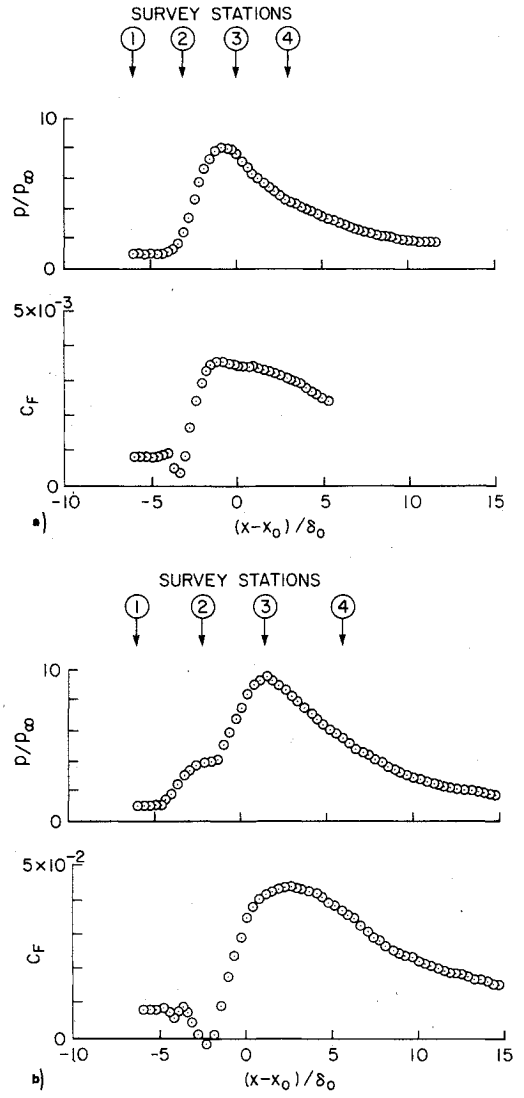

Fig. 3 a) Surface pressure and skin friction distributions for attached flow ($\alpha = 7.5°$). b) Surface pressure and skin friction distributions for separated flow ($\alpha = 15°$).

C. Turbulence Measurements

The turbulent fluctuations were measured with specially designed dual hot-wire probes free of strain-gaging and wire oscillations. The details of the probe design and construction procedures are presented in Ref. 7. The probe consisted of two 10-μm-diam platinum-rhodium wires mounted on a ceramic wedge. The overall probe diameter was 0.24 cm. The wires were operated using constant temperature anemometers at an overheat ratio near 1.0 where it has been shown[7,8] that the wires are solely mass-flux sensitive for the present flow conditions. The upper frequency limit (−3 dB) of the probes, as determined by the conventional square-wave technique, was approximately 100 kHz. The probes were calibrated by comparing their RMS-outputs to the previously measured mass-flux intensities[7,8] obtained for the present flowfield upstream of the interaction region using conventional hot wires. The flow quantities measured were $\langle(\rho u)'\rangle$, $\langle v'\rangle$, and $R_{(\rho u)'v'}$. The Reynolds shear stress $\overline{(\rho u'v')}$ was deduced from these measurements using the method outlined in Sec. III.

Hot-wire surveys through the boundary layer (at vertical intervals of 0.125 cm) were obtained at 4 axial locations for both the attached and separated flowfields. The axial location for each run was established prior to the run by prepositioning the shock generator. Figure 3 shows the mean surface measurements[4] obtained for two shock-wave generator angles

and the location of the survey stations. The first set of measurements corresponded to the upstream undisturbed boundary layer, the second set to the locations of minimum skin friction for the attached case and the middle of the separated bubble for the separated case, the third set to the peak pressure location, and the fourth set to a location several boundary-layer thicknesses downstream. The data presented only include results were a single probe survived 4 consecutive runs at the 4 axial survey stations for each flowfield.

III. Equations for Turbulent Shear Stress

To obtain the Reynolds shear stress $\rho\,\overline{u'v'}$ from hot-wire measurements for compressible turbulent flows, the assumption that the pressure vertical-velocity correlation $\overline{p'v'}$ is equal to zero must be made. The resulting expression for shear stress is[7]

$$\bar{\rho}\,\overline{u'v'} = \frac{c_p T}{c_p \tilde{T} + \tilde{u}^2}\left(\overline{(\rho u)'v'} + \frac{\overline{u\rho}}{\bar{T}}\,\overline{T_t'v'}\right) \tag{1}$$

where the cross-correlations $\overline{(\rho u)'v'}$ and $\overline{T_t'v'}$ are measured quantities using either the mode diagram or the direct measurement technique. Since the measurement of the term $\overline{T_t'v'}$ is highly questionable using a constant temperature anemometer,[8] and extremely tedious using constant current anemometers with a modal analysis, an alternate approach for obtaining Reynolds shear stress is proposed. This approach assumes a known turbulent Prandtl number in addition to a zero-pressure vertical-velocity correlation, but only requires a single measurement of the cross-correlation $\overline{(\rho u)'v'}$ provided the hot wires are operated at a high enough overheat to make them solely sensitive to mass-flux fluctuations.[7,8]

The cross-correlation $\overline{(\rho u)'v'}$ can be expanded as follows

$$\overline{(\rho u)'v'} = \bar{\rho}\,\overline{u'v'} + \tilde{u}\overline{\rho'v'} + \text{higher order correlations} \tag{2}$$

Then, expanding the equation of state, multiplying by v', time-averaging, and assuming zero correlation between pressure and vertical-velocity fluctuations, we obtain a relation between density and temperature correlations with velocity

$$\overline{p'v'} = 0 = R(\tilde{T}\overline{\rho'v'} + \bar{\rho}\,\overline{T'v'}) \tag{3}$$

The turbulent Prandtl number is defined

$$Pr_t = \frac{\overline{u'v'}\,\mathrm{d}\tilde{T}/\mathrm{d}y}{\overline{T'v'}\,\mathrm{d}\tilde{u}/\mathrm{d}y} \tag{4}$$

Expanding the energy equation

$$\mathrm{d}\tilde{T}_t/\mathrm{d}y = \mathrm{d}\tilde{T}/\mathrm{d}y + \frac{\tilde{u}}{c_p}\,\mathrm{d}\tilde{u}/\mathrm{d}y \tag{5}$$

Combining Eqs. (3-5) and recalling that $\tilde{u}^2/c_p\tilde{T} = (\gamma-1)M^2$ we obtain

$$\tilde{u}\overline{\rho'v'} = \bar{\rho}\,\overline{u'v'}\,\frac{(\gamma-1)M^2}{Pr_t}\left(1 - \frac{c_p}{\tilde{u}}\,\frac{\mathrm{d}\tilde{T}_t/\mathrm{d}y}{\mathrm{d}\tilde{u}/\mathrm{d}y}\right) \tag{6}$$

Substituting Eq. (6) into Eq. (2), the equation for Reynolds shear stress becomes

$$\bar{\rho}\,\overline{u'v'} = \left[1 + \frac{(\gamma-1)M^2}{Pr_t}\left(1 - \frac{c_p\,\mathrm{d}\tilde{T}_t/\mathrm{d}y}{\tilde{u}\,\mathrm{d}\tilde{u}/\mathrm{d}y}\right)\right]^{-1}\overline{(\rho u)'v'} \tag{7}$$

For adiabatic flow this relation reduces to

$$\bar{\rho}\,\overline{u'v'} = \left[1 + \frac{(\gamma-1)M^2}{Pr_t}\right]^{-1}\overline{(\rho u)'v'} \tag{8}$$

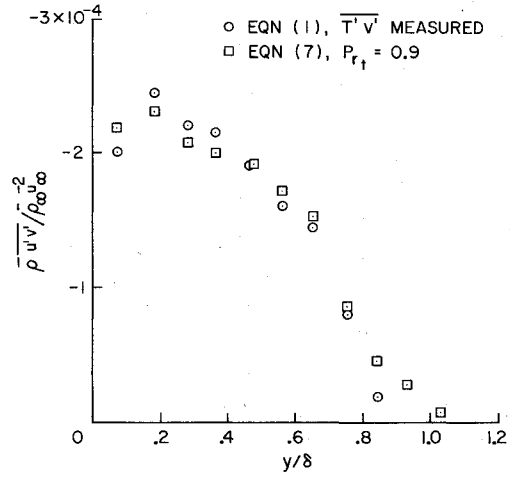

Fig. 4 Comparison of Reynolds shear stress distributions using two deduction techniques.

Equation (7) was used to deduce the Reynolds shear stress from the present measurements assuming $Pr_t = 0.9$; the results are discussed in Sec. IV.

To test the turbulent Prandtl number assumption, the deduced shear stress distributions across an equilibrium hypersonic boundary layer[7] are compared in Fig. 4; they are calculated using Eq. (1) with the measured value of $\overline{T_t'v'}$ and using Eq. (7) with $Pr_t = 0.9$. The two methods give excellent agreement. For the present nonequilibrium flow where Pr_t may deviate from 0.9, a 10% error in Pr_t results in a 5% error in shear stress in the inner half of the boundary layer and up to a 10% error in shear stress near the boundary-layer edge. Values of Pr_t obtained from the integration of the mean momentum and energy equations using the measured mean profiles[4] indicate that Pr_t varies from 0.6 to 1.2 for the present nonequilibrium flows. Since these calculated values are only approximate due to the uncertainties in determining derivatives of experimental data, an average value, $Pr_t = 0.9$, was used for the present measurements.

IV. Results and Discussion

To verify conventional eddy viscosity turbulence models, the variation of Reynolds shear stress must be measured throughout the flowfield. For higher order models, additional fluctuating measurements such as turbulent kinetic energy are required. The present measurements include the Reynolds shear stress as well as the fluctuating mass-flux and vertical-velocity intensities, which should be indicative of the turbulent kinetic energy per unit mass. Also included are estimates of the turbulent lifetimes for these quantities.

A. Turbulent Intensities

Measurements of the rms mass-flux $\langle (\rho u)' \rangle$ and vertical-velocity $\langle v' \rangle$ fluctuations across the boundary layer are shown for the attached and separated flows in Figs. 5 and 6, respectively. First, for the attached flow case, there is a significant increase in both $\langle (\rho u)' \rangle$ and $\langle v' \rangle$ at station 2 due to the shock wave impingement. The rms mass flux fluctuations exceed 40%. For these large turbulent intensities the interaction between the 3 turbulent velocity components, as well as the density and pressure fluctuations, are important. Since correction procedures to account for these interactions require extensive measurements of third- and fourth-order correlations,[9] no corrections have been applied to the present data. For incompressible jet flows with rms velocity fluctuations the same order as the present measurements, these corrections were determined to be as high as 20%.[9] The corrected values can either be higher or lower than the measured values, depending on the signs of the higher-order correlations. As opposed to the intensity distribution in the undisturbed boundary layer, the peak value occurs away from the wall, as expected for adverse pressure gradients. At the

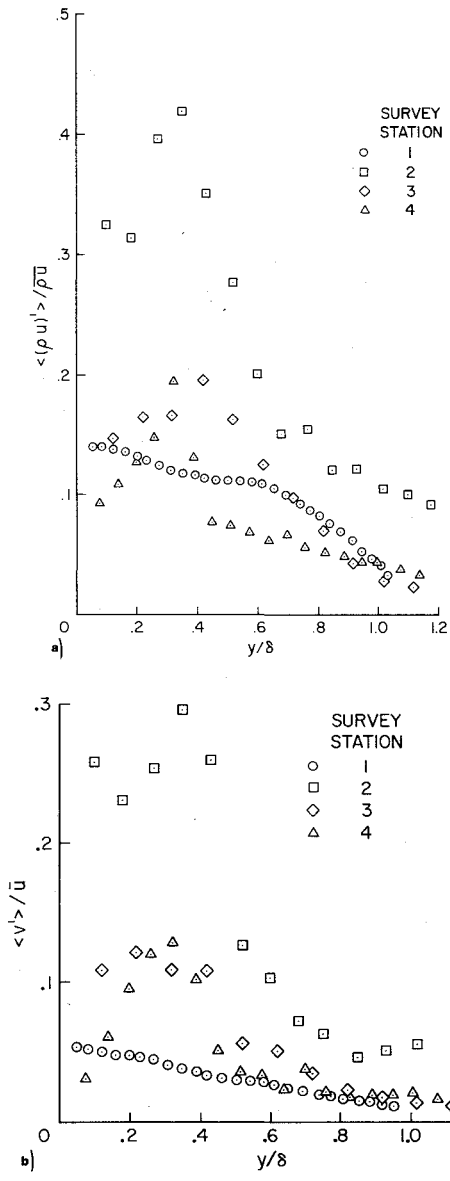

Fig. 5 a) rms mass-flux distributions, attached flow. b) rms vertical-velocity distributions, attached flow.

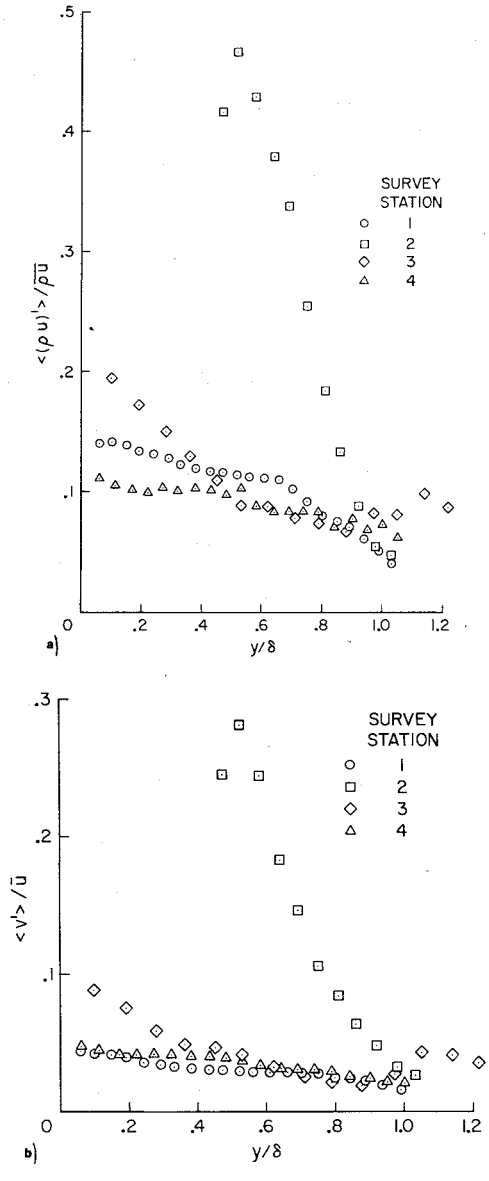

Fig. 6 a) rms mass-flux distributions, separated flow. b) rms vertical-velocity distributions, separated flow.

downstream locations the magnitudes of the fluctuations are diminished but are still significantly greater than the upstream undisturbed values in the inner half of the boundary layer. Also, the high intensity away from the wall still persists at the downstream stations even in zero or favorable pressure gradient flow.

For the separated flow case (Fig. 6), a similar increase in both $\langle(\rho u)'\rangle$ and $\langle v'\rangle$ is observed at station 2 due to shock wave impingement. The magnitude of the rms mass flux fluctuations approaches 50%. This location coincides with the center of the separated zone. Data are not presented near the wall in the reversed flow region ($0<y/\delta<0.25$) or in the region immediately above due to the low wire Reynolds numbers which were beyond the calibration range of the probes. At the two downstream locations, the magnitudes of the fluctuations are significantly reduced and are in close agreement with the upstream equilibrium values with the maximum fluctuations occurring at the wall and continuously decreasing away from the wall. On comparing the attached and separated cases, significant differences are noted. While the magnitudes of the fluctuations are similar at the second location, the data at the two downstream locations indicate higher fluctuations at the wall for the separated case; however, away from the wall ($y/\delta\approx0.3$), the attached case shows mass-flux fluctuation magnitudes a factor of two greater than the separated case, and vertical velocity-fluctuations magnitudes are a factor of three greater. In the outer half of the boundary layer, the intensities are similar for the two cases at the two downstream stations. The implication is that the separation process either destroys turbulence memory or inhibits production of turbulence with a new equilibrium-type boundary layer originating near reattachment; this effect is opposed to that seen in the attached case, where the approach to equilibrium flow is more gradual.

B. Turbulent Reynolds Stresses

The Reynolds shear stress distributions deduced using Eq. (7) with Pr_t are shown in Fig. 7 for the attached and separated flows. The solid symbols denote the measured shear stress at the wall obtained from a floating element balance.[4] In general, the shear stress distributions show the same trends as the fluctuating intensities previously discussed. At the second location the shear distributions are similar for the two flows (the separated case is displaced outward due to the separation bubble) and indicate typical distributions for adverse pressure gradient flows. However, at the third location the two flows again show large differences, although the values of surface skin friction are almost equal. The attached flow distribution

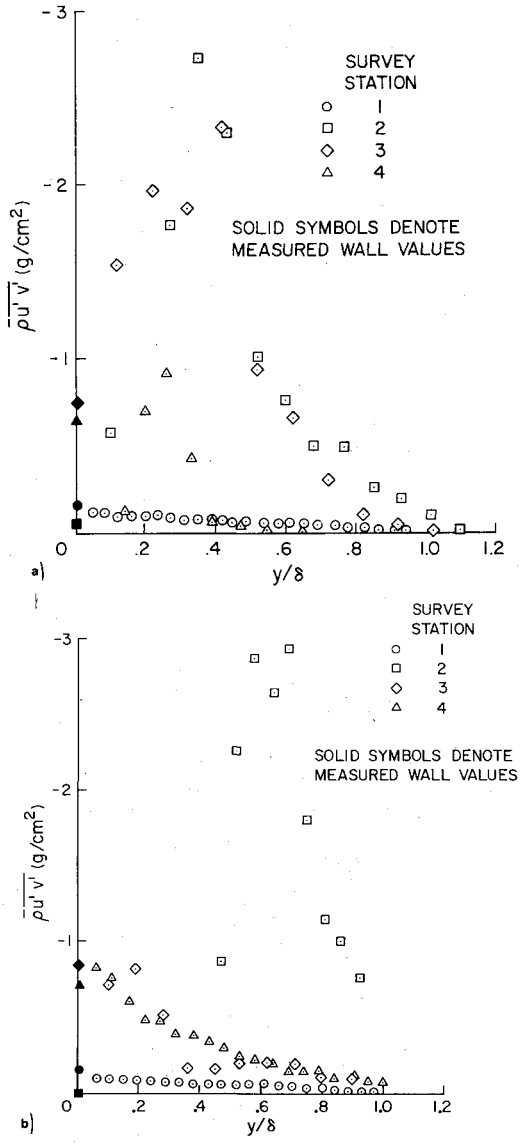

Fig. 7 a) Reynolds shear stress distributions, attached flow. b) Reynolds shear stress distributions, separated flow.

displays large turbulent memory effects in that it is still typical of an adverse pressure gradient flow, although the surface pressure gradient is zero at this location. At the fourth location for the attached case, the shear distribution has relaxed somewhat, but is still not typical of a favorable pressure gradient flow where the shear is a maximum at the wall. For the separated case (Fig. 7b) the shear distributions for the third and fourth locations resemble equilibrium distributations for a zero and favorable pressure gradient flow, respectively, with the maximum value occurring near the wall.

A comparison of the measured shear stress distributions and those obtained from the integration of the mean momentum equation using the measured mean flow profiles[4] are shown in Fig. 8 for both flowfields. For the attached case (Fig. 8a), the results from the two methods are in reasonable agreement, considering the possible errors involved.[4,7] For the separated case (Fig. 8b), the agreement is again reasonable except for the third survey location where an order-of-magnitude difference exists between the two methods. Reasons for this disagreement could be the boundary-layer assumption employed for the integral method which is invalid near separation, or the $\overline{\rho' v'} = 0$ assumption used to deduce the hot-wire shear stress which is probably most critical in this region. However, since the rms mass-flux and vertical-velocity fluctuations were also much lower for the separated

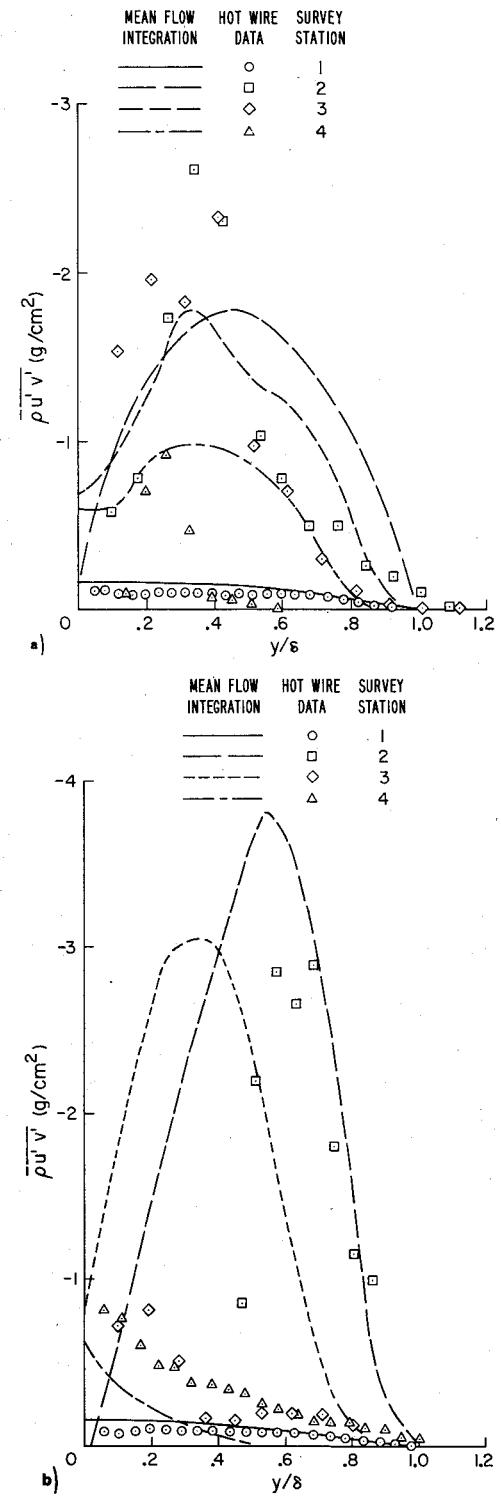

Fig. 8 a) Comparison of the measured Reynolds shear stress distributions with values obtained from integration of the mean momentum equation, attached flow. b) Comparison of the measured Reynolds shear stress distributions with values obtained from integration of the mean momentum equation, separated flow.

case at this location, the measured trend in the hot-wire shear distributions should be more correct.

C. Statistical Properties in the Turbulent Fluctuations

To gain additional insight into the effect of boundary-layer separation on the fluctuating quantities, detailed power-spectral-density distributions were obtained throughout both flowfields. Normalized power spectra of the vertical-velocity fluctuations for the four survey stations on a streamline originating at $y/\delta = 0.15$ at station 1 are shown in Fig. 9 for

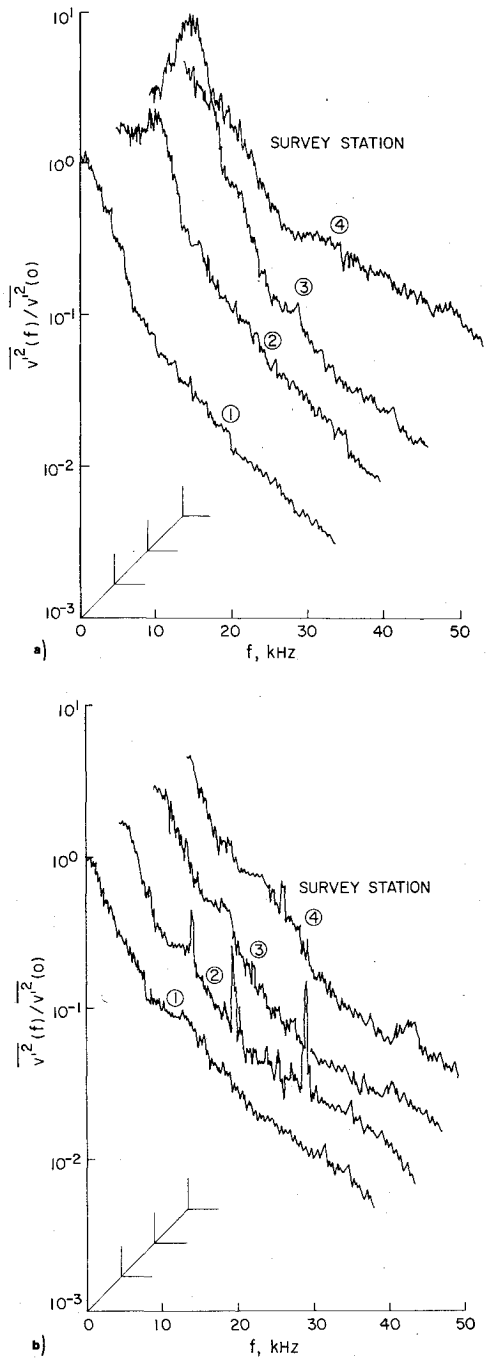

Fig. 9 a) Normalized power spectra of the vertical-velocity fluctuations, attached flow ($\alpha = 7.5°$). b) Normalized power spectra of the vertical-velocity fluctuations, separated flow ($\alpha = 15°$).

the attached and separated flowfields. Several interesting features can be noted from these data. First it is seen that the spectral distributions for the two flow fields are significantly different in that the attached flow results indicate an increase in the percentage of turbulent energy at frequencies above 5 kHz for the 3 downstream stations. Initially this increase is concentrated at frequencies between 5 and 10 kHz at stations 2 and 3. At station 4 the increase has shifted to frequencies above 20 kHz, indicating the transfer of the turbulence to smaller scales as the flow proceeds downstream. Although the initial spectra for the separated case (station 1) shows an increased energy content at the higher frequencies when compared to the attached case, the three downstream locations have essentially the same spectra as the first station except for the peaks in the spectrum at station 2. (The differences in the initial spectra for the two cases is a result of the differences in initial boundary-layer thicknesses.) These peaks (located at 10, 15, and 25 KHz) are associated with the unsteadiness of the separation bubble and closely agree with the energy peaks observed for this same flow field obtained using surface thin-film gauges.[10] Similar peaks were observed for other streamlines up to values of $y/\delta = 0.7$ at this station. Since the dominant frequencies of the separation bubble unsteadiness occur over the same frequency range as the increase in turbulent energy observed for the attached case, this result suggests a possible physical mechanism for the lack of increase in turbulent energy for the separated case as opposed to the attached case. That is, the coupling of the unsteady nature of the separation bubble with the turbulent energy field removes the energy from the turbulent field that was induced by the shock-wave impingement. This effect in turn permits the boundary layer downstream of the interaction to relax to an equilibrium state much faster in the separated case than in the attached case. Spectra obtained for streamlines further away from the wall, and of the mass flux fluctuations, show similar trends.

A direct confirmation of the cross coupling of the shear stress energy and the bubble unsteadiness is shown in Fig. 10 where power spectra for the cross-correltion $(\rho u)'v'$ and its two components are shown for several positions across the boundary layer at the third survey location for the separated flow. This location is approximately four boundary-layer thicknesses downstream of the reattachment point. The spectra for the cross-correlations were obtained from Fourier transforms of the cross-correlation functions. Although the individual components $(\rho u)'$ and v' have smoothly varying spectra, the cross-correlations show large dips in their spectra for $y/\delta \approx 0.15$. These dips, or losses in energy, occur at exactly the same frequencies as the peaks in the v' spectra at the previous station due to the bubble unsteadiness. This result shows a direct coupling between these two modes of energy. This effect implies that the bubble unsteadiness creates a cross-correlation $\overline{(\rho u)'v'}$ of opposite sign to the shear stress, thus canceling the increased shear resulting from adverse pressure gradient before it is convected downstream. At the fourth survey location these dips were no longer present. In fact, for both flows this was the only survey location where these dips were observed in the cross-correlation spectra.

D. Turbulence Lifetimes

Although the axial survey locations for the present study were spaced at intervals too large to obtain accurate data concerning the various turbulence lifetimes, there are sufficient data to obtain rough estimates. Referring to Figs. 5 and 6, and recalling that station 3 corresponds to a zero axial pressure gradient flow and station 4 to a favorable pressure gradient flow for both cases, the turbulent intensities are still out of equilibrium at station 4 for the attached case, and close to equilibrium at station 3 for the separated case. In terms of average boundary-layer thicknesses, the turbulence lifetime for turbulent intensities can be estimated in excess of 14 boundary-layer thickness for the attached flow and on the order of 5 for the separated flow. The Reynolds shear stress distribution at station 4 for the attached case (see Fig. 8a) is apparently approaching equilibrium slightly faster than the turbulent intensities, which suggests a smaller turbulence lifetime for the shear stress than the kinetic energy. Verification of this effect would require more detailed measurements.

V. Conclusions

This report presents new quantitative turbulence data for two shock-wave boundary-layer interaction flowfields, one with separation and one without. For the first time, a direct comparison has been made to determine the influence of separation and separation bubble unsteadiness on the turbulent intensities and shear distributions after reattachment of a separated boundary layer. Comparison of the separated and attached flows has shown a significant increase in turbulent intensities and Reynolds shear stress downstream of

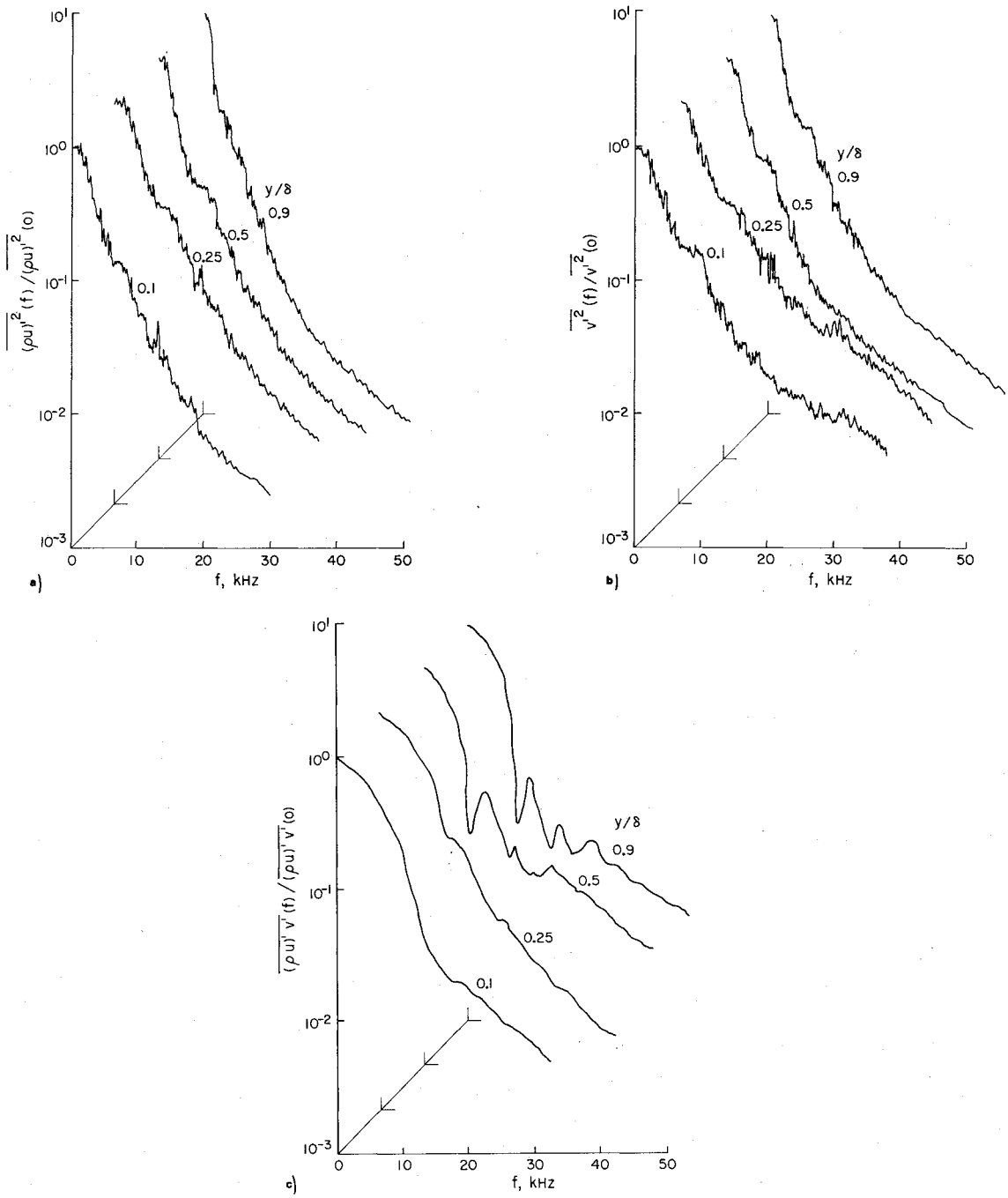

Fig. 10 a) Normalized power spectra at survey station 3, separated flow; mass-flux fluctuations. b) Normalized power spectra at survey station 3, separated flow; vertical-velocity fluctuations, c) Normalized power spectra at survey station 3, separated flow; mass-flux vertical-velocity cross-correlation.

the interaction region for the attached case, while for the separated case the increases were insignificant. For the attached case the increased turbulent energy because of shock-wave impingement persists at least 15 boundary-layer thicknesses downstream, while for the separated case the flowfield returns to equilibrium conditions much faster. A similar trend but with slightly smaller lifetimes was observed for the shear stress. A possible explanation for these differences is a coupling between the turbulent energy and the separation bubble unsteadiness which results in the dissipation of the turbulent energy. The statistical properties of the turbulent fluctuations support this hypothesis.

It has also been demonstrated that the new specially developed hot-wire probes designed to operate at extremely high overheats without sacrificing strength can provide previously unattainable turbulence measurements in nonadiabatic hypersonic interactions flows. By using a new approximation (assuming a turbulent Prandtl number), shear stress data were obtained from a single dual wire measurement. The measurements were in reasonable agreement with shear-stress distributions obtained by integrating the momentum equation, except near the reattachment region for the separated boundary-layer flow.

References

[1] Shang, J.S. and Hankey, W.L., *Supersonic Turbulent Separated Flows Utilizing the Navier Stokes Equations,* AGARDograph-CPP-168, 1975.

[2] Baldwin, B.S. and Rose, W.C., "Calculation of Shock-Separated Turbulent Boundary Layers," NASA Conference on Aerodynamic Analyses Requiring Advanced Computers, Langley Research Center, Hampton, Va., NASA SP-347, March 1975.

[3]Wilcox, D.C., "Numerical Study of Separated Turbulent Flows," *AIAA Journal,* Vol. 13, May 1975, pp. 555-556.

[4]Marvin, J.G., Horstman, C.C., Rubesin, M.W., Coakley, T.J., and Kussoy, M.I., "An Experimental and Numerical Investigation of Shock-Wave Induced Turbulent Boundary-Layer Separation at Hypersonic Speeds," AGARDograph-CPP-168, May 1975.

[5]Baldwin, B.S. and MacCormack, R.W., "Numerical Solution of Interaction of a Strong Shock Wave with a Hypersonic Turbulent Boundary Layer," AIAA Paper 74-558, Palo Alto, Calif., 1974.

[6]Rose, W.C. and Johnson, D.A., "Turbulent in a Shock-Wave Boundary-Layer Interaction," *AIAA Journal,* Vol. 13, July 1975, pp. 884-889.

[7]Mikulla, V. and Horstman, C.C., "Turbulence Stress Measurements in a Nonadiabatic Hypersonic Boundary Layer,"*AIAA Journal,* Vol. 13, Dec. 1975, pp. 1607-1613.

[8]Owen, F.K., Horstman, C.C., and Kussoy, M.I., "Mean and Fluctuating Flow Measurements of a Fully-Developed, Non-Adiabatic Hypersonic Boundary Layer," *Journal of Fluid Mechanics,* Vol. 70, Part 2, July 1975, pp. 393-413.

[9]Guitton, D.E., "The Effect of High Intensity Turbulence on the Response of a Hot Wire," *Transactions, CASI,* Vol. 7, 1974, pp. 69-80.

[10]Horstman, C.C. and Owen, F.K., "New Diagnostic Technique for the Study of Turbulent Boundary-Layer Separation," *AIAA Journal,* Vol. 12, Oct. 1974, pp. 1436-1438.